Rapidity distributions of dileptons from a hadronizing quark-gluon plasma

R. Vogt
Gesellschaft für Schwerionenforschung (GSI), D-6100 Darmstadt 11, Germany

B. V. Jacak and P. L. McGaughey
Los Alamos National Laboratory, Los Alamos, New Mexico 87545

P. V. Ruuskanen
Research Institute for Theoretical Physics, University of Helsinki, P.O. Box 9, FIN-00014 Helsinki, Finland
and Department of Physics, University of Jyväskylä, P.O. Box 35 FIN-40351 Jyväskylä, Finland

(Received 7 September 1993)

It has been predicted that dilepton production may be used as a quark-gluon plasma probe. We calculate the rapidity distributions of thermal dileptons produced by an evolving quark-gluon plasma assuming a longitudinal scaling expansion with initial conditions locally determined from the hadronic rapidity density. These distributions are compared with Drell-Yan production and semileptonic charm decays at invariant mass $M=2$, 4, and 6 GeV.

PACS number(s): 12.38.Mh, 25.75.+r

One of the challenges in ultrarelativistic heavy-ion physics is to differentiate the thermal signatures of a quark-gluon plasma from particles produced in the initial nucleon-nucleon interactions. In order for dilepton production to be a useful plasma probe one must then distinguish between thermal production and the significant "background" dilepton production from initially produced Drell-Yan and charm pairs. We focus on the rapidity distributions of lepton pairs in the mass region between $2 \le M \le 6$ GeV where thermal production could be competitive with initial dilepton production. We also show that thermal charm production is significant.

The rapidity distribution of Drell-Yan pairs of invariant mass M in central (impact parameter $b=0$) AA interactions, averaged over protons and neutrons, is defined as

$$\frac{dN}{dM\,dy}=\frac{A^{4/3}}{\pi r_0^3}K\frac{8\pi\alpha^2}{9M^3}\{\tfrac{5}{18}[x_a v(x_a)x_b s(x_b)+x_a s(x_a)x_b v(x_b)+4x_a s(x_a)x_b s(x_b)]+\tfrac{4}{18}x_a s(x_a)x_b s(x_b)\}\,, \quad (1)$$

where $K=2$ accounts for higher-order corrections, $v(x)=u_v(x)+d_v(x)$ is the valence quark distribution, and $s(x)=2[\bar{u}(x)+\bar{d}(x)+\bar{s}(x)]/6$ is the average sea quark distribution in a nucleon assuming a flavor symmetric sea. We have used the new lowest-order set of structure functions, Duke-Owens set 1.1 [1], in our calculations. The fractions of the initial projectile and target momenta carried by the interacting partons are given by $x_a=Me^{y}/\sqrt{s}$ and $x_b=Me^{-y}/\sqrt{s}$, respectively.

The rapidity distributions from Drell-Yan production in a central Au+Au collision are shown in Fig. 1(a) for energies reached at the Brookhaven Relativistic Heavy Ion Collider (RHIC) and Fig. 1(b) for the CERN Large Hadron Collider (LHC). At RHIC, the rate rises slightly for $M=2$ GeV and stays fairly constant over three units of rapidity even for $M=6$ GeV. It drops off steeply at the kinematic limit. At the LHC, the rate rises somewhat over four units of rapidity for all masses. This effect is most prominent at the LHC for $M=2$ GeV where $x_b \le 0.000\,32$ and $x_a \ge 0.000\,32$. The sea-sea term in Eq. (1) is the dominant contribution and increases slightly since x_b remains near the small-x limit of the structure functions while x_a increases with y. The first sea-valence contribution in Eq. (1) increases with y but the second decreases because a small decrease in x_b leads to a fast decrease of $x_b v(x_b)$. Thus, the total Drell-Yan rate increases with y by $\approx 30\%$.

The charmed hadron production cross section in a nucleon-nucleon collision is [2,3]

$$E_3E_4\frac{d\sigma}{d^3p_3d^3p_4}=K\int\frac{\hat{s}}{2\pi}\frac{dx_a}{x_a}\frac{dx_b}{x_b}dz_3dz_4H(x_a,x_b)\frac{E_3E_4}{E_1E_2}\times\frac{D(z_3)D(z_4)}{z_3^3z_4^3}\delta^4(p_a+p_b-p_1-p_2)\,, \quad (2)$$

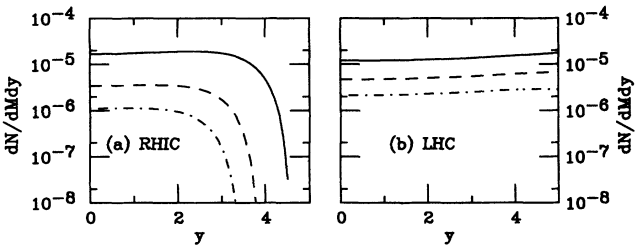

FIG. 1. Rapidity distributions of Drell-Yan pairs at $M=2$ (solid), 4 (dashed), and 6 (dot-dashed) GeV in a central Au+Au collision at (a) RHIC and the (b) LHC.

where subscripts a and b represent the incoming partons, 1 and 2, the charmed quarks. and 3 and 4, the charmed hadrons. The function $D(z)$ describes the fragmentation of the charmed quarks into hadrons. In Ref. [2] it was shown that charm hadroproduction is best described by the assumption that the charmed quark loses no momentum during hadronization, i.e., $D(z)=\delta(1-z)$. Given this, e.g., $p_{\parallel_1}=p_{\parallel_3}$, but $y_1\neq y_3$. (A fragmentation function assuming some momentum loss results in a more central rapidity distribution.) The convolution function $H(x_a,x_b)$ is

$$H(x_a,x_b)=\sum_{n_f}[x_a q_{n_f}(x_a)x_b\bar{q}_{n_f}(x_b)+x_a\bar{q}_{n_f}(x_a)x_b q_{n_f}(x_b)]\frac{d\hat{\sigma}}{d\hat{t}}\bigg|_{q\bar{q}}+x_a g(x_a)x_b g(x_b)\frac{d\hat{\sigma}}{d\hat{t}}\bigg|_{gg}, \tag{3}$$

where $q(x)$ and $g(x)$ are the parton distributions [1]. For the explicit subprocess cross sections, see, e.g., Ref. [4].

We assume no intrinsic p_T for the light quarks and use four-momentum conservation to integrate over x_a and x_b. Then the number of charmed hadrons produced in a central AA collision is

$$\frac{dN}{dM_{D\bar{D}}dy_{D\bar{D}}}=\frac{A^{4\alpha/3}}{\pi r_0^2}2K\int dp_T^2 dz_3 dz_4 dy_3 dy_4 M_{D\bar{D}}H(x_a,x_b)\frac{E_3E_4}{E_1E_2}\frac{D(z_3)D(z_4)}{z_3z_4}$$
$$\times\delta(y_{D\bar{D}}-(y_3+y_4)/2)\delta(M_{D\bar{D}}^2-(p_3+p_4)^2), \tag{4}$$

where $M_{D\bar{D}}$ and $y_{D\bar{D}}$ are the mass and rapidity of the $D\bar{D}$ pair. The uncertainty in the magnitude of the charm production cross section from a lowest-order calculation results in $K\sim 2-3$. The shape of the rapidity distribution is relatively unaffected by next-to-leading-order corrections [5]. Since pA measurements [6–8] indicate $\alpha\sim 0.9-1$, we use $\alpha=1$ to give an upper bound on initial charm production. Using Eq. (4), we can determine the rapidity distribution of lepton pairs from the decay $D\bar{D}\rightarrow l^+l^-$ + anything and from the average branching ratio $B(D/D^*\rightarrow l^+ + \text{anything})\sim 12\%$. [$B(D^0\rightarrow l^+ + \text{anything})=7.7\%$ and $B(D^+\rightarrow l^+ + \text{anything})=19.3\%$ while $D^{0*}\rightarrow D^0X$ and $D^{+*}\rightarrow D^+/D^0X$, where X is either a photon or pion.] Given a $D\bar{D}$ pair with mass and rapidity distributed according to Eq. (4), the decay to dileptons is performed. The pair is first assigned a transverse momentum and polar angle using a parametrization of the charm pair correlation data of Ref. [9]. Then the two D's are semileptonically decayed according to the lepton energy spectrum reported in Ref. [10]. At high energies and for large nuclei more than one $D\bar{D}$ pair may be produced so that the detected charm decay leptons may be uncorrelated.

The charmed hadron rapidity distributions are shown in Figs. 2(a) and 2(b) for Au+Au collisions at RHIC and LHC (solid curves) along with the resulting lepton pair distributions at $M=2$ (dashed), 4 (dot-dashed), and 6 (dotted) GeV (scaled up by 100 to fit on the same plot). Charm decays are copious at these energies ($\sigma_{D\bar{D}}\sim 190$ μ b at RHIC and 1.95 mb at LHC using $m_c=1.5$ GeV and $K=2$, compatible with the next-to-leading-order results [5]). Measurements suggest that charm decays are important in the dilepton spectrum at $M=2$ GeV at CERN Super Proton Synchrotron (SPS) energies [11,12]. Fermilab experiment E789 at 800 GeV observed that the dilepton continuum at $M<M_{J/\psi}$ is much greater than expected from Drell-Yan pairs alone, indicating that the dominant background may be due to charm decays [13]. A judicious choice of kinematic cuts can reduce the charm acceptance relative to that of Drell-Yan pairs. Drell-Yan pairs are produced with equal but opposite transverse momentum with $p_T<M$ while the transverse momenta of the leptons from charm decays are only weakly correlated. This is discussed in more detail below.

We have not included shadowing of the nuclear structure functions in our calculation. Shadowing would lead

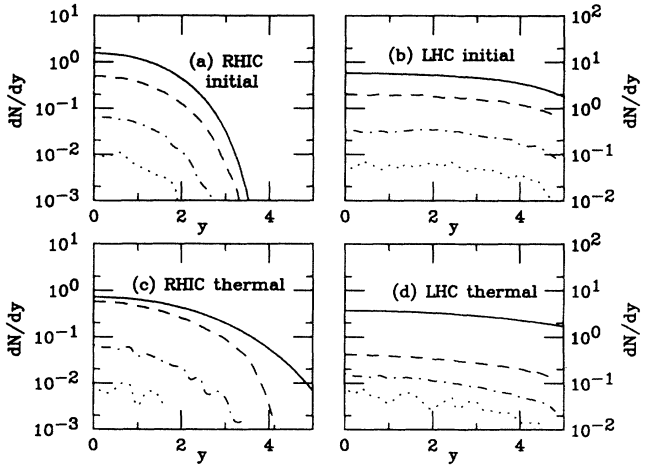

FIG. 2. Initially produced charmed pair distributions (solid curves) from a central Au+Au collision at (a) RHIC and at the (b) LHC. Also shown are the lepton pair distributions resulting from semileptonic decays of charm at $M_{D\bar{D}}=2$ (dashed), 4 (dot-dashed), and 6 (dotted) GeV. The lepton pairs from the decays have been scaled up by a factor of 100. Thermal charm production is shown in (c) at RHIC and (d) at the LHC. The decay leptons from thermal charm at RHIC are scaled up by a factor of 1000 for $M=2$ GeV (dashed), 10^4 at $M=4$ GeV (dot-dashed), and 10^5 at $M=6$ GeV (dotted). At the LHC, the decays with $M=2$ GeV are scaled up by 100 while those with $M=4$ (dot-dashed) and $M=6$ GeV (dotted) are scaled up by 1000 and 10 000.

to a depletion of both the charm and Drell-Yan cross sections in the very low x_b region. The effect is strongest at small y since both the beam and target distributions are shadowed, leading to a faster increase of the Drell-Yan rate with y. Aside from the uncertainties in the rates due to shadowing, it is important to note that the nucleon structure functions have not yet been measured in the LHC x region and are also not well known for RHIC. The DESY ep collider HERA will study the region $10^{-5} \leq x$ and $Q^2 > 10$ GeV^2. Since extrapolations of the measured structure functions to the low-x region differ widely, the HERA results could, by favoring some models over others, lead to significant changes in the calculations of $\sigma_{\rm DY}$ and $\sigma_{D\bar{D}}$. For example, using Kiewicinski-Martin-Roberts-Stirling set B0 (KMRS B0) [14], a higher-order set of structure functions with a larger sea quark contribution at low x, increases the Drell-Yan cross section by a factor of 2. Early results from HERA favor sea quark and gluon distributions that increase as $x \to 0$, suggesting that, particularly at LHC energies, QCD calculations are quite sensitive to the choice of structure functions [15].

Thus far we have been considering the expected background to the thermal dileptons, now we discuss the signal itself. At RHIC and LHC it is reasonable to expect the longitudinal expansion to approximately follow the scaling law, $v_z = z/t$. This assumption must break down at large rapidities where particle densities become small. There, in the fragmentation regions, pressure gradients become significant, matter is accelerated, and the longitudinal velocity, even if initially given by $v_z = z/t$, will later deviate from the scaling law. Numerical calculations [16,17] give support for a picture where these deviations are small up to the fragmentation regions and we will neglect them here. We will comment on their effect when discussing the results.

With the scaling ansatz for the longitudinal velocity we can relate the initial density to the final multiplicity distribution of hadrons by $n_i \tau_i = (dN/d\eta)/(\pi R_A^2)$. The temperature is therefore a function of η, $T_i \equiv T_i(\eta)$ where we can identify the fluid and particle rapidities since the overall rapidity distribution is much broader than the thermal distribution at freezeout. The multiplicity distribution is parametrized as

$$\frac{dN}{d\eta} = \left[\frac{dN}{d\eta}\right]_0 \exp(-\eta^2/2\sigma^2) , \tag{5}$$

where $(dN/d\eta)_0$ is the total multiplicity at $\eta = 0$ and σ is the width. At RHIC energies, $|\eta| \leq 6$ and we choose $(dN/d\eta)_0 = 2000$ while for the LHC $|\eta| \leq 8$ and we take $(dN/d\eta)_0 = 5000$. To estimate σ we calculate the total energy of the final particles taking $\langle m_T \rangle \simeq 0.5$ GeV and integrating the Gaussian shape to the kinematical limit. At RHIC the collision energy is reproduced for $\sigma \sim 3$ and at LHC for ~ 5. Like the scaling properties of the longitudinal velocity, the Gaussian form of the multiplicity distribution must break down at rapidities close to the phase-space limit. There, however, the densities become too small for thermal production to be observed.

The dilepton emission rate is [18,19]

$$\frac{dN}{d^4x\, d^2p_T dy\, dM^2} = \frac{\alpha^2}{8\pi^4} F \exp\{-[m_T \cosh(y-\eta)/T]\} , \tag{6}$$

where M, p_T, m_T, and y are the mass, transverse momentum, transverse mass, and rapidity of the pair and η is the rapidity of the medium with temperature T. In a plasma, $F_Q = \sum e_q^2$, while in an equilibrium hadron gas, assuming $\pi\pi \to \rho \to l^+ l^-$ is the dominant channel, $F_H = \frac{1}{12} m_\rho^4 / [(m_\rho^2 - M^2)^2 + m_\rho^2 \Gamma_\rho^2]$. Neglecting other processes may underestimate the emission from the hadron gas which could affect the low-mass results. The mixed phase has a fractional contribution from each. After integration over p_T, τ, and transverse area, the rapidity distribution for a given dilepton mass is

$$\begin{aligned}\frac{dN}{dM\,dy} = \frac{\alpha^2}{2\pi^3}\pi R_A^2 \Bigg\{ & \theta(s_i - s_Q)\frac{3F_Q}{M^3}\int_{-Y}^{Y} d\eta (\tau_i T_i^3)^2 \frac{x^4+5x^3+15x^2+30x+30}{\cosh^6(\eta - y)} e^{-x}\Big|_{x_c}^{x_i} \\ & + \theta(s_i - s_H) M^3 \frac{\tau_m^2}{2} f_0 (r-1)\{f_0 F_Q + [(r-2)f_0 + 2]F_H\} \int_{-Y}^{Y} d\eta \left[\frac{1}{x_c} + \frac{1}{x_c^2}\right] e^{-x_c} \\ & + \theta(s_i - s_{\rm dec})\frac{3F_H}{M^3}\int_{-Y}^{Y} d\eta (\tau_H T_H^3)^2 \frac{x^4+5x^3+15x^2+30x+30}{\cosh^6(\eta - y)} e^{-x}\Big|_{x_{\rm dec}}^{x_H} \Bigg\} ,\end{aligned} \tag{7}$$

where $x = M\cosh(\eta - y)/T$, s_i is the initial entropy density, and s_Q and s_H are the entropy densities of the plasma and the hadron gas at the transition temperature T_c.

We neglect the transverse expansion and describe the properties of the matter in the longitudinal direction only. Transverse expansion mainly affects the hadron gas phase and the later part of the mixed phase [20,21]. If the transverse expansion is included, the contribution from the hadron gas phase is negligible for $M \geq 2$ GeV except at large rapidities where the initial density is too low to produce a plasma.

As defaults, we assume a three-flavor plasma and a hadron gas of massless pions with $T_c = 200$ MeV and $T_{\rm dec} = 140$ MeV. Then

$$s_i = \begin{cases} 4\gamma_k \dfrac{\pi^2}{90} T_i^3 , & s_i > s_Q \text{ or } s_i < s_H , \\ f_0 s_Q + (1-f_0) s_H , & s_H < s_i < s_Q , \end{cases}$$

where γ_k is the number of degrees of freedom with $\gamma_H=3$ and $\gamma_Q=16+21n_f/2$ and $n_i=s_i/3.6$. The beginning of the mixed phase occurs at

$$\tau_m=\begin{cases}\tau_i(T_i/T_c)^3\ , & T_i>T_c\ ,\\ 1\text{ fm}\ , & T_i=T_c\ .\end{cases}$$

The initial plasma content of the mixed phase is

$$f_0=\begin{cases}1\ , & T_i>T_c\ ,\\ (s_i-s_H)/(s_Q-s_H)\ , & T_i=T_c\ ,\\ 0\ , & T_i<T_c\ .\end{cases}$$

The beginning of the hadron phase is then

$$\tau_H=\begin{cases}\tau_m r\ , & T_i\geq T_c\ ,\\ 1\text{ fm}\ , & T_i<T_c\ ,\end{cases}$$

where $r=s_Q/s_H=\gamma_Q/\gamma_H$. There is no thermal contribution if $T_i<T_{\rm dec}$.

We have used three different hypotheses to fix T_i and τ_i. First we assume a fixed initial time, $\tau_i\equiv 1$ fm. We then define $dN/d\eta|_Q=\pi R_A^2 n_Q\tau_i$, $dN/d\eta|_H=\pi R_A^2 n_H\tau_i$, and $dN/d\eta|_{\rm dec}=\pi R_A^2 n_{\rm dec}\tau_i$. If $dN/d\eta>dN/d\eta|_Q$ the system begins in the plasma phase and

$$T_i=\left\{\frac{dN}{d\eta}\frac{T_c^3}{\pi R_A^2 n_Q\tau_i}\right\}^{1/3}\ . \tag{8}$$

If $dN/d\eta|_H<dN/d\eta<dN/d\eta|_Q$, the system begins in the mixed phase. If $dN/d\eta|_{\rm dec}<dN/d\eta<dN/d\eta|_H$, it begins in the hadron gas with

$$T_i=T_H=\left\{\frac{dN}{d\eta}\frac{T_c^3}{\pi R_A^2 n_H\tau_i}\right\}^{1/3}\ . \tag{9}$$

There is no contribution if $dN/d\eta<dN/d\eta|_{\rm dec}$. The maximum initial temperature $T_{i,\max}$ obtained with a fixed initial time is the lowest of all three hypotheses. In this case we find $T_{i,\max}\sim 255$ MeV at RHIC and 350 MeV at the LHC.

As an alternative way of determining the initial time τ_i and temperature T_i, we use the bound $\tau_i\langle E_i\rangle\simeq 3\tau_i T_i=C\geq 1$ from the uncertainty relation. We consider two cases, $C=3$ and 1, where the latter gives an absolute lower bound on τ_i and an upper bound on T_i. Recent results from the parton cascade model [22] and estimates of gluon thermalization [23] give some support for a short formation time. In this case, the initial temperature of the plasma is

$$T_i=\left\{\frac{dN}{d\eta}\frac{3T_c^3}{\pi R_A^2 n_Q C}\right\}^{1/2}\ . \tag{10}$$

If $T_i\leq T_c$, then the formation time is again fixed to be $\tau_i=1$ fm and the system begins in the mixed phase or hadron gas, according to the multiplicity, as before. When $C=3$, we find $T_{i,\max}\sim 300$ MeV at RHIC and 465 MeV at the LHC. Using $C=1$, we have $T_{i,\max}\sim 515$ and 810 MeV, respectively, similar to the results of Ref. [24]. The corresponding values of τ_i are ~ 0.2 and 0.08 fm, respectively. These low values of $\tau_{i,\min}$ may simulate preequilibrium pair production where the initial parton distributions evolve into thermal distributions [25,26].

In Fig. 3 we show thermal dilepton production at RHIC for $M=2$ GeV [Figs. 3(a) and 3(b)], $M=4$ GeV [Figs. 3(c) and 3(d)], and $M=6$ GeV [Figs. 3(e) and 3(f)]. The full evolution (plasma, mixed phase, and hadron gas) is shown in Figs. 3(a), 3(c), and 3(e) while the plasma contribution alone is given in Figs. 3(b), 3(d), and 3(f). The thermal dilepton distributions arising from the fixed initial time with T_i from Eq. (8) (solid) and the uncertainty bound from Eq. (10) with $C=3$ (dashed) and $C=1$ (dot-dashed) are given. Dilepton production by the plasma is most important at central rapidities where the initial temperature is greatest. Including the mixed phase and the hadron gas broadens the rapidity distributions. Without transverse expansion, the lifetime of the hadron gas phase at central rapidities, where the initial density is high, becomes very long (of order 80 fm when $T_i\sim T_{i,\max}$) and its contribution to the thermal pair rate $dN/dM\,dy$ is thus unphysically large. At higher rapidities, the calculated hadron contribution is more physical since the initial density is too low to form a plasma and the effects of transverse expansion remain small. In Figs. 3(a), 3(c), and 3(e) the thermal dilepton distributions merge at

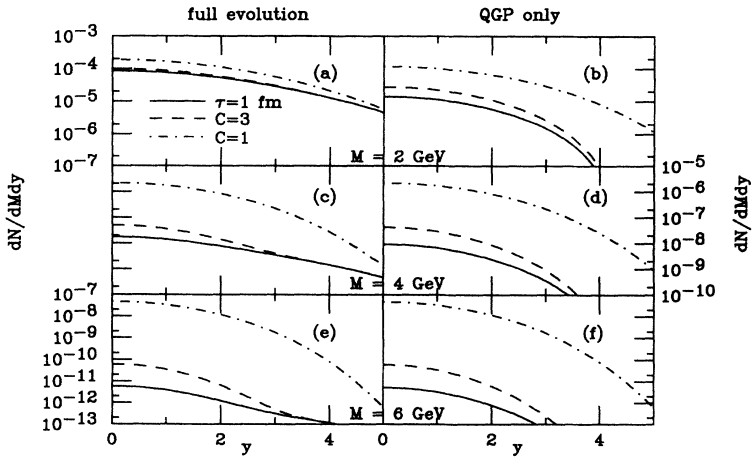

FIG. 3. The rapidity distribution of thermal dileptons produced at RHIC with $\sigma=3$ in Eq. (5) are shown for (a) and (b) $M=2$ GeV, (c) and (d) $M=4$ GeV, and (e) and (f) $M=6$ GeV. The thermal curves represent the three choices of τ_i and T_i, $\tau_i\equiv 1$ fm (solid), $C=3$ (dashed), and $C=1$ (dot-dashed). The full evolution (plasma, mixed phase, and hadron gas) is given in (a), (c), and (e) while the plasma contribution alone is shown in (b), (d), and (f).

higher rapidities since $\tau_i \equiv 1$ fm where $T_i \leq T_c$. Later time contributions are less important when $C=1$ because of the high $T_{i,\max}$. The distributions from plasma alone, Figs. 3(b), 3(d), and 3(f), are narrower and have a reduced yield. Since it is difficult to produce high-mass pairs when $T_i \leq T_c$, at $M=6$ GeV the yield at $y=0$ is unchanged in Figs. 3(e) and 3(f). The results for the LHC are given in Fig. 4. Due to the increased $T_{i,\max}$, the contribution from the plasma dominates the thermal emission for $M>2$ GeV at this energy. To show the most optimistic results of thermal dilepton production, we will compare the $C=1$ curves with the other contributions to the dilepton spectrum. One must keep in mind, however, that the other choices of initial conditions result in a much smaller thermal yield for $M>2$ GeV.

We have also varied our inputs to see how the rapidity distributions are affected. Increasing the effective number of hadron degrees of freedom through the presence of additional thermal mesons [21,27] decreases the lifetime of the mixed phase and hadron gas, leading to a smaller hadronic contribution to the evolution. Changing to a two-flavor plasma increases the initial temperature considerably. For $\tau_i \equiv 1$, $T_{i,\max}$ grows to 285 MeV at RHIC and 386 MeV at the LHC. When $C=3$, we have 340 and 540 MeV while when $C=1$, we find 590 and 930 MeV, respectively. Setting $T_c=140$ MeV and $T_{\rm dec}=100$ MeV increases τ_m but results in a decrease of the mixed phase and hadron contributions due to the larger x_c and $x_{\rm dec}$ (lower T_c and $T_{\rm dec}$) in Eq. (7).

If $C=1$ represents the more physical situation, one might expect a significant amount of thermal charm production since $T_{i,\max} \sim (\frac{1}{3}-\frac{1}{2})m_c$. The importance of thermal charm production has previously been suggested [23,28]. For completeness, we also estimate the rapidity distribution of dileptons from thermal charm production. The thermal $c\bar{c}$ production rate is

$$\frac{dN}{d^4x} = \int \frac{d^3k_a}{(2\pi)^3} f(k_a) \frac{d^3k_b}{(2\pi)^3} f(k_b) \sigma_{c\bar{c}}(M) v_{\rm rel} , \quad (11)$$

where $v_{\rm rel}$ is the relative velocity of the thermal partons, $v_{\rm rel} = \sqrt{(k_a \cdot k_b)^2 - m_q^4}/(E_a E_b)$. We use a Boltzmann distribution for the incoming partons, as before. Following Ref. [28], we write the charm production cross section as

$$\sigma_{c\bar{c}}(M) = \gamma_q \sigma_{q\bar{q}\to c\bar{c}}(M) + \gamma_g \sigma_{gg\to c\bar{c}}(M) , \quad (12)$$

where the quark and gluon degeneracy factors are $\gamma_q = 3\times(2\times3)^2$ for three quark flavors and $\gamma_g = (2\times8)^2/2$ (the factor of $\frac{1}{2}$ is to prevent double counting) [28]. The cross sections are given in Ref. [29]. We consider only production from the plasma phase for this case since the later stages of evolution do not have sufficiently high temperatures to provide significant thermal charm production. We have not included charm fragmentation since this has only a minor effect on the rapidity distribution as compared to that of the source. Therefore, we may simply write

$$\frac{dN}{dM\,dy} = \frac{3\sigma_{c\bar{c}}(M)}{4M(2\pi)^4} \pi R_A^2 \theta(s_i - s_Q) \int_{-Y}^{Y} d\eta (\tau_i T_i^3)^2 \frac{x^4+5x^3+15x^2+30x+30}{\cosh^6(\eta - y)} e^{-x}\Big|_{x_c}^{x_i} . \quad (13)$$

The resulting distributions are similar in shape to the thermal dileptons but broader than the initial charm production. Thermal charm production is comparable to that in the initial nucleon-nucleon interactions. In Figs. 2(c) and 2(d) we compare the thermal and initial charm production. The mass distribution is much steeper for the thermal production, resulting in a smaller decay contribution at higher masses. For comparison, at RHIC, the $M=2$-GeV curve is multiplied by a factor of 1000 while the $M=4$- and 6-GeV results are multiplied by 10^4 and 10^5, respectively. At the LHC, the multipliers are 100 for $M=2$ GeV, 1000 for $M=4$, and 10^4 for $M=6$ GeV.

Our combined results for lepton pairs with $M=2$, 4, and 6 GeV are given in Figs. 5 and 6 at RHIC and LHC, respectively. The Drell-Yan and initial charm contribu-

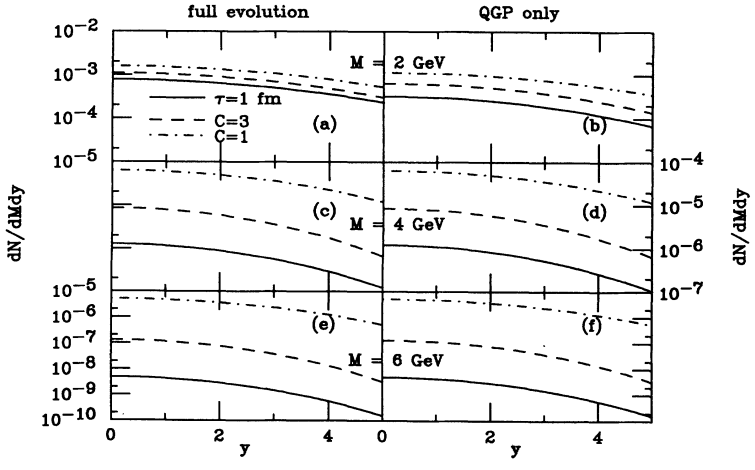

FIG. 4. The same as Fig. 3 for the LHC with $\sigma=5$.

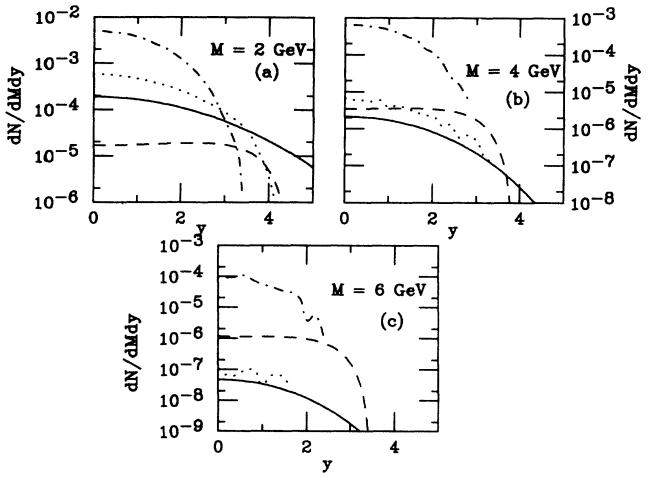

FIG. 5. We compare the contributions to the dilepton spectrum at RHIC for (a) $M=2$ GeV, (b) $M=4$ GeV, and (c) $M=6$ GeV. Drell-Yan (dashed), direct thermal dileptons with $C=1$ (solid), thermal (dotted) and initial (dot-dashed) charm production are included.

tions are given by the dashed and dot-dashed curves. The thermal dileptons arising from direct production over the full time evolution and charm decays produced by plasma only with $C=1$ are given by the solid and dotted curves. The thermal dileptons have the broadest distribution of all the contributions at RHIC while the decays of initially produced charm have the narrowest. The slopes are also somewhat different near the central region. At $M=2$ GeV, the thermal contributions are above the Drell-Yan contribution. At the LHC, the thermal rate remains compatible with the Drell-Yan yield and all the slopes are similar. However, at $y>3$ the thermal and charm decay contributions are decreasing while the Drell-Yan rate is still increasing.

Although the initial charm contribution is very large, it may be possible to separate it from the thermal dilepton and Drell-Yan contributions. At RHIC, $e\mu$ coincidence measurements could prove useful. Charm was

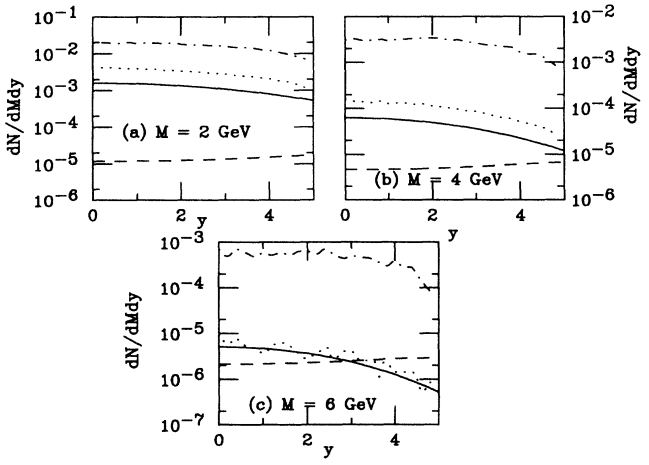

FIG. 6. The same as in Fig. 5 for the LHC.

TABLE I. Acceptance in PHENIX muon arm for dileptons from various sources at $y=2$.

Mass	2 GeV	4 GeV	6 GeV
Drell-Yan	3.9%	5.4%	4.6%
Thermal dileptons	4.9	6.8	5.8
Charm decays	0.88	0.89	0.25

first measured by this method at the CERN Intersecting Storage Rings (ISR) [30] and such coincidence measurements are planned at RHIC [31]. Opposite sign $e\mu$ pairs from decay of two charmed particles are correlated if only one $D\bar{D}$ pair is produced in an event, which is the case for pp and light-ion collisions at RHIC. If $\alpha=1$ in Eq. (4), up to five primary $D\bar{D}$ pairs could be produced in Au+Au collisions, yielding uncorrelated $e\mu$ pairs. The production rate of Drell-Yan pairs and thermal dileptons is much less than one pair per event so uncorrelated $e\mu$ production from these processes is very unlikely. However, thermal charm may be important if the thermalization time is short, and cause significant additional production of uncorrelated $e\mu$ pairs. Pairs of like-sign electrons may offer a better measure of charm production if more than two $D\bar{D}$ pairs are produced per event. This is probable for all ion species in the LHC environment, where $e\mu$ coincidence measurements will not be possible in any case [32].

Figures 5 and 6 suggest a very large correction to the measured dilepton distributions if subtraction of the charm contribution is attempted. However, these figures do not include the experimental acceptance, smaller for leptons from charm decay than for Drell-Yan or thermal dileptons. Table I shows the acceptances in the muon channel of the RHIC PHENIX detector at $M=2$, 4, and 6 GeV and $y=2$. The Drell-Yan and thermal acceptances are from 4 to 20 times larger than for the charm decay leptons [31]. Consequently, the thermal and Drell-Yan contributions do not represent only a few percent of the total dilepton yield and subtraction of the charm contribution may thus be feasible. This is illustrated in Table II which shows the ratios of the cross sections without, then with, the effects of acceptance. It is important to note that in the case of dileptons from uncorrelated charm decays, the acceptance drops by anoth-

TABLE II. The upper section gives the ratio of dileptons produced by other sources to Drell-Yan production at RHIC. The lower section shows the effect of the PHENIX muon acceptance on these ratios at $y=2$.

Mass	2 GeV	4 GeV	6 GeV
Ratio of dilepton source to Drell-Yan Production			
Thermal ($C=1$)	6.1	0.25	0.013
Charm	66	33	3.8
Thermal charm	14	0.73	0
Acceptance correction included			
Thermal ($C=1$)	7.7	0.31	0.016
Charm	15	5.5	0.21
Thermal charm	3.1	0.12	0

er factor of nearly 2 due to the larger rapidity difference between the leptons. It should be possible to optimize a rapidity cut to further discriminate against dileptons from uncorrelated charm. Whether such a cut can be used to reject a majority of the combinatorial lepton pairs from uncorrelated charm can only be addressed for specific detector geometries.

If it is possible to reliably remove the charm decay contributions to the dileptons, the significant differences between the rapidity distributions of thermal and Drell-Yan dileptons could be measured. The Drell-Yan contribution grows slightly with y while the thermals decrease with y. Since the expansion accelerates the matter also in the longitudinal direction a full hydrodynamic calculation would give a narrower rapidity distribution for the thermally emitted pairs than the one which we obtained here with the time-independent scaling approximation for the longitudinal velocity. Also the correlation of thermal production with the hadronic multiplicity and the effect of shadowing on Drell-Yan pairs should lead to opposite trends in the mass number dependence of these two contributions. Stronger shadowing for higher-mass nuclei favors the larger-y region for Drell-Yan pairs. Increasing the mass number should narrow the rapidity distribution due to the stronger stopping and consequently also narrow the thermal dilepton distribution. The shape of the distributions in the central several units of rapidity should thus provide an indication of the dilepton source. A significantly broad rapidity and mass coverage at RHIC and LHC would allow such a study.

In summary, we have calculated the rapidity distributions of dilepton production from various sources in heavy-ion collisions at RHIC and LHC. The calculated distributions cover four or more units of rapidity, suggesting the contributions to dilepton measurements over a wide range of rapidities. A large experimental rapidity coverage is desirable to allow a search for variations in the shape of the dilepton rapidity distributions in pp, pA, and AA collisions. Charmed particle decays into leptons are very important, but the kinematics of the charm decays differ from that of thermal or Drell-Yan dilepton production. Consequently the acceptance of realistic detectors makes the charm background which must be subtracted to study the thermal dileptons more tractable. Furthermore the significant production of thermal charm may offer a novel way to study the collisions, since the rate is comparable to direct thermal dileptons. Experiments could search for broadening of the dilepton distribution in AA collisions after fixing the level of charm production in pp interactions.

We would like to thank S. Gavin and G. Young for useful discussions. R.V. thanks Los Alamos National Laboratory and the University of Jyväskylä for their hospitality.

[1] J. F. Owens, Phys. Lett. B **266**, 126 (1991).
[2] R. Vogt, S. J. Brodsky, and P. Hoyer, Nucl. Phys. **B383**, 643 (1992).
[3] S. Banerjee and S. N. Ganguli, Phys. Rev. D **33**, 1278 (1986).
[4] R. K. Ellis, in *Physics at the 100 GeV Scale,* Proceedings of the 17th SLAC Summer Institute, Stanford, California, 1989, edited by E. C. Brennan (SLAC Report No. 361, Stanford, 1990).
[5] M. Mangano, P. Nason, and G. Ridolfi, Nucl Phys. **B373**, 295 (1992); M. Mangano, P. Nason, and G. Ridolfi, *ibid.* **B405**, 507 (1993).
[6] M. J. Leitch (private communication).
[7] J. A. Appel, Annu. Rev. Nucl. Part. Sci. **42**, 367 (1992).
[8] G. A. Alves *et al.*, Phys. Rev. Lett. **70**, 722 (1993).
[9] K. Kodama *et al.*, Phys. Lett. B **263**, 579 (1991).
[10] R. M. Baltrusaitis *et al.*, Phys. Rev. Lett. **54**, 1976 (1985).
[11] HELIOS Collaboration, M. A. Mazzoni, in *Quark Matter '93,* Proceedings of the International Conference on Ultrarelativistic Nucleus-Nucleus Collisions, Börlange, Sweden, 1993 (unpublished).
[12] C. Lourenco, in *Quark Matter '93* [11].
[13] M. J. Leitch, in *Quark Matter '91,* Proceedings of the Ninth International Conference on Ultrarelativistic Nucleus-Nucleus Collisions, Gatlinburg, Tennessee, edited by T. C. Awes *et al.* [Nucl. Phys. **A544**, 197c (1992)].
[14] J. Kiewicinski, A. D. Martin, R. G. Roberts, and W. J. Stirling, Phys. Rev. D **42**, 3645 (1990).
[15] L. Jönnson, in *Quark Matter '93* [11].
[16] K. Kajantie, R. Raitio, and P. V. Ruuskanen, Nucl. Phys. **B222**, 152 (1983).
[17] M. Kataja, Z. Phys. C **38**, 419 (1988).
[18] K. Kajantie and P. V. Ruuskanen, Z. Phys. C **44**, 167 (1989).
[19] M. I. Gorenstein and O. P. Pavlenko, Z. Phys. C **37**, 611 (1988).
[20] P. V. Ruuskanen, Z. Phys. C **38**, 219 (1988).
[21] M. Kataja, J. Letessier, P. V. Ruuskanen, and A. Tounsi, Z. Phys. C **55**, 153 (1992).
[22] K. Geiger, Phys. Rev. D **47**, 133 (1993).
[23] E. Shuryak, Phys. Rev. Lett. **68**, 3270 (1992).
[24] J. I. Kapusta, L. McLerran, and D. K. Srivastava, Phys. Lett. B **283**, 145 (1992).
[25] K. Geiger and J. I. Kapusta, Phys. Rev. Lett. **70**, 1920 (1993).
[26] D. Seibert and T. Altherr, Phys. Rev. D **48**, 3386 (1993).
[27] D. K. Srivastava *et al.*, Phys. Lett. B **276**, 285 (1992).
[28] A. Shor, Phys. Lett. B **215**, 375 (1988); A. Shor, *ibid.* **233**, 231 (1989).
[29] B. L. Combridge, Nucl. Phys. **B151**, 429 (1979).
[30] A. G. Clark *et al.*, Phys. Lett. **77B**, 339 (1978); A. Chilingarov *et al.*, *ibid.* **83B**, 136 (1979).
[31] PHENIX Conceptual Design Report, 1993 (unpublished).
[32] ALICE Letter of Intent, CERN Report No. CERN/LHCC/93-16, 1993 (unpublished).